Published in final edited form as:

Cell Rep. 2018 December 04; 25(10): 2784–2796.e3. doi:10.1016/j.celrep.2018.11.030.

ISRE-Reporter Mouse Reveals High Basal and Induced Type I IFN Responses in Inflammatory Monocytes

Melissa B. Uccellini[1] and **Adolfo García-Sastre**[1,2,3,4,*]

[1]Department of Microbiology, Icahn School of Medicine at Mount Sinai, New York, NY, USA

[2]Department of Medicine, Division of Infectious Diseases, Icahn School of Medicine at Mount Sinai, New York, NY, USA

[3]Global Health and Emerging Pathogens Institute, Icahn School of Medicine at Mount Sinai, New York, NY, USA

[4]Lead Contact

SUMMARY

Type I and type III interferons (IFNs) are critical for controlling viral infections. However, the precise dynamics of the IFN response have been difficult to define *in vivo*. Signaling through type I IFN receptors leads to interferon-stimulated response element (ISRE)-dependent gene expression and an antiviral state. As an alternative to tracking IFN, we used an ISRE-dependent reporter mouse to define the cell types, localization, and kinetics of IFN responding cells during influenza virus infection. We find that measurable IFN responses are largely limited to hematopoietic cells, which show a high sensitivity to IFN. Inflammatory monocytes display high basal IFN responses, which are enhanced upon infection and correlate with infection of these cells. We find that inflammatory monocyte development is independent of IFN signaling; however, IFN is critical for chemokine production and recruitment following infection. The data reveal a role for inflammatory monocytes in both basal IFN responses and responses to infection.

Graphical Abstract

*Correspondence: adolfo.garcia-sastre@mssm.edu.

AUTHOR CONTRIBUTIONS

M.B.U. conceived the project, performed the experiments, generated the figures, and wrote the manuscript. A.G.-S. conceived the project, supervised the work, provided funding, and critically reviewed the manuscript.

SUPPLEMENTAL INFORMATION

Supplemental Information includes five figures and one table and can be found with this article online at https://doi.org/10.1016/j.celrep.2018.11.030.

DECLARATION OF INTERESTS

The authors declare no competing interests.

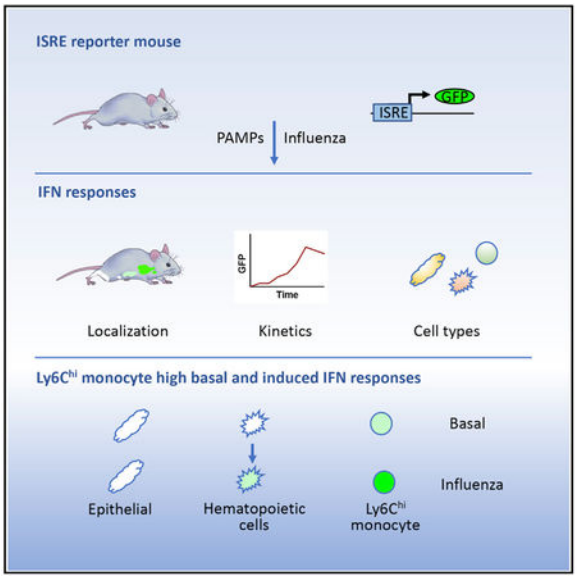

In Brief

Uccellini and García-Sastre create an ISRE reporter mouse and track interferon (IFN) responses *in vivo* in response to pathogen-associated molecular pattern (PAMP) stimulation and influenza infection. They find that IFN responses are highest in hematopoietic cells during infection. Specifically, Ly6C^{hi} inflammatory monocytes have high basal IFN responses that are further enhanced upon infection.

INTRODUCTION

Detection of virus by the innate immune system triggers the production of type I (α/β) and type III interferon (IFN) (λ), which serve as a critical first line of defense against infection. *Ifnb1*, and murine *Ifna4* in certain cell types, are transcribed in an initial IRF3- dependent burst, triggering the production of IRF7, which leads to a subsequent secondary wave of transcription involving the other *Ifna* genes (Honda et al., 2005). IFN-α/β binds to the heterodimeric type I IFN receptor composed of IFNAR1 and IFNAR2, which is expressed on all nucleated cells. IFN-λ binds to the type III IFN receptor composed of IL-28Rα and IL-10Rβ. Expression of IL-28Rα is more restricted and thought to be mainly on epithelial cells (Pott et al., 2011; Sommereyns et al., 2008). Canonical signaling through both the type I and type III IFN receptors leads to the activation of JAK1 and TYK2, the phosphorylation of STAT1 and STAT2, and their binding to IRF9 to form interferon-stimulated gene factor 3 (ISGF3). Binding of ISGF3 to interferon-stimulated response elements (ISREs) leads to the activation of hundreds of IFN-stimulated genes (ISGs), which act through diverse mechanisms to limit viral replication and create an antiviral state. IFN-α/β can also signal through STAT1 homodimers, which bind to γ-activated sequences (GASs), through other STATs, and through the phosphatidylinositol 3-kinase and mitogen-activated protein kinase (MAPK) signaling pathways (Ivashkiv and Donlin, 2014). Besides its antiviral activity, IFN signaling has been associated with both pro- and anti-inflammatory activities, most likely reflecting cell-type-specific responses to IFN.

The importance of IFN *in vivo* was demonstrated by the high susceptibility of *Ifnar1*$^{-/-}$ mice to many viruses, supporting a critical role for type I IFN in limiting viral replication and dissemination (Müller et al., 1994). While IFN is critical for control of many viral infections, its role in influenza virus infection is less clear, likely due to a degree of redundancy between the functions of IFN-α/β and -λ, variation in mouse strains, and variation in viral strains. IFN can act at many different levels on a broad range of cell types to influence the outcome of influenza virus infection; appropriate amounts of IFN appear to be protective, while excessive amounts contribute to tissue damage (McNab et al., 2015). Both IFN-α/β and IFN-λ can induce the expression of Mx1, which is a primary restriction factor for influenza virus infection in mice (Mordstein et al., 2010). Most standard laboratory mouse strains lack expression of functional Mx1 (Staeheli et al., 1988), which has led to differing conclusions about the protective versus pathogenic functions of IFN during infection. However, in Mx-sufficient strains, a critical function of IFN is induction of Mx1, which cripples viral replication and subsequent downstream inflammation. Because of a degree of redundancy between type I and III IFN on cells that express both receptors, both *Ifnar1*$^{-/-}$ and *Il28ra*$^{-/-}$ mice show little phenotype on an Mx1-sufficient background; however, the absence of both receptors leads to significantly higher viral titers and enhanced susceptibility to mortality (Mordstein et al., 2008). Both IFN-α/β and IFN-λ can also act to induce the expression of other ISGs, including ISG15, PKR, PAI1, IFITM3, and IRF7, which act through a variety of mechanisms to limit viral replication (Ciancanelli et al., 2016). Type I IFN also plays a role in limiting the dissemination of certain strains of influenza virus. Most influenza virus strains require proteolytic cleavage of hemagglutinin by trypsin-like proteases expressed in the lung; however, some human strains such as 1918, A/WSN/33, and highly pathogenic avian viruses can replicate independently of trypsin, allowing spread outside of the lung (Steinhauer, 1999).*Ifnar1*$^{-/-}$ mice are more susceptible to these strains, suggesting that IFN-α/β can act in a manner that is not complemented by IFN-λ to limit viral dissemination (García-Sastre et al., 1998a; Salomon et al., 2007; Szretter et al., 2009). Both IFN-α/β and IFN-λ also play important roles in inducing chemokines that serve to recruit inflammatory cells to the site of infection (Rauch et al., 2013).

While IFN is critical for controlling viral infection, a lack of sensitive detection systems has limited our understanding of the precise mechanisms by which it functions *in vivo*. IFN can be quantified at the protein level by ELISA or bioassay; however, these assays have a low sensitivity. A recently described assay using single-molecule array digital ELISA technology shows a 5,000-fold increase in sensitivity over commercial ELISAs (Rodero et al., 2017). IFN can also be measured at the RNA level by RT-PCR or RNA sequencing (RNA-seq), methods that have a high sensitivity. Nevertheless, these methods do not provide information about the cell types producing IFN unless combined with cell sorting. To address this, a number of reporter mouse strains have been generated, including a mouse expressing YFP from an IRES in the *Ifnb1* gene (Scheu et al., 2008), a mouse with luciferase replacing the *Ifnb1* gene (Lienenklaus et al., 2009), and a mouse expressing GFP from an IRES in the *Ifna6* gene, which is expressed during the secondary wave of IFN production (Kumagai et al., 2007). During non-inflammatory conditions, thymic epithelial cells show high basal expression of the IFN-β reporter (Lienenklaus et al., 2009). Under infection conditions,

these models have revealed different cellular sources of IFN. While the different studies used different markers to define cell populations, it appears that during systemic infection, plasmacytoid dendritic cells (pDCs) and macrophages in the spleen are the main IFN producers, whereas respiratory infection leads to IFN production mainly in macrophage subsets (Barbalat et al., 2009; Dresing et al., 2010; Goritzka et al., 2015; Jung et al., 2008; Kim et al., 2012; Scheu et al., 2008; Solodova et al., 2011). Reporter mice infected with influenza virus show strong tissue-specific IFN-β production associated with areas of active viral replication (Lienenklaus et al., 2009). IFN-β induction correlated with the ability of the virus to productively replicate in the lung (Kochs et al., 2009). The viral IFN antagonist protein NS1 plays an important role in delaying the expression of IFN-β and restricting the cell types that express it. Infection with wild-type (WT) strains leads to IFN production in cells of the macrophage/dendritic cell (DC) lineage, while mutant strains are able to induce IFN production in epithelial cells (Kallfass et al., 2013; Lienenklaus et al., 2009).

While these studies have revealed the IFN producing cells, many questions remain about the activity of IFN after secretion, including the extent to which it stays local or causes a systemic response under different conditions, the localizations, and cell types that respond, and the kinetics of the response. To address some of these questions, Pulverer created a bacterial artificial chromosome/clone (BAC) transgenic mouse that expresses luciferase under the control of the *Mx2* promoter, which revealed a surprisingly strong IFN response in the liver (Pulverer et al., 2010). The luciferase reporter allows imaging on a whole animal level but is not amenable to tracking individual cells. Here, we have created a reporter mouse expressing GFP under the control of the endogenous *Mx1* locus. Mx1 is induced by type I and III IFN, but not by type II IFN or other cytokines (Haller and Kochs, 2011), and is strictly controlled by ISGF3 binding to its ISRE and therefore serves as a reporter for the canonical IFN signaling pathway (Mordstein et al., 2010). Using this model, we find that during influenza virus infection, IFN responses remain locally confined, are delayed in terms of kinetics, and are largely restricted to hematopoietic cells. We also find a previously unreported role for monocytes in both high basal and induced IFN responses. Type I IFN has been suggested to be required for the generation and differentiation of $Ly6C^{hi}$ monocytes (Seo et al., 2011). Here we show that both $Ly6C^{hi}$ and $Ly6C^{lo}$ monocytes are present in mice deficient for IFN signaling, although their recruitment is severely reduced as reported (Seo et al., 2011). Importantly, the monocyte chemokines CCL2 and CCL7 are ISGs and are not induced in the absence of IFN signaling, which likely accounts for the failure to recruit monocytes in the absence of IFN signaling.

RESULTS

Mx1^{gfp} Reporter Mice

In order to study the cells responding to IFN *in vivo*, we generated a reporter mouse expressing GFP under the control of the endogenous *Mx1* locus. Because the C57BL/6 strain lacks a functional *Mx1* gene (Staeheli et al., 1988), as do most inbred laboratory strains, inclusion of GFP does not have a functional impact on this strain. A GFP-ovalbumin (OVA) fusion protein was inserted into the *Mx1* locus (Figure S1A). OVA epitopes were included to track T cell responses, which will be reported elsewhere. Correct integration of

the construct into the *Mx1* locus was confirmed (Figures S1B and S1C). To confirm IFN inducibility of the reporter, bone-marrow-derived macrophages from $Mx1^{gfp}$ mice were stimulated with IFN or infected with virus and GFP expression was examined. As expected, $Mx1^{gfp}$ macrophages expressed GFP following treatment with type I IFN or infection with PR8 influenza virus (Figure S1D). Infection with PR8DNS1 virus (García-Sastre et al., 1998b) induced GFP expression in a larger proportion of cells than the WT virus (Figure S1D). In order to confirm that GFP expression faithfully reflected *Mx1* expression, we performed intracellular staining for Mx1 and GFP in $Mx1^{gfp}/Mx1^{+}$ heterozygous mice (from the B6.A2G-$Mx1^{+}$ congenic line); however, GFP fluorescence was lost upon permeablization for staining (data not shown) as reported by others (Kalejta et al., 1997). We therefore injected $Mx1^{gfp}/Mx1^{+}$ mice intravenously (i.v.) with Poly(I:C) (PIC) and sorted GFP^{-} and GFP^{+} cells from the spleen. *Mx1* expression was enriched in the GFP^{+} cells relative to the GFP^{-} cells (Figure S1E). Overall the data confirm that the $Mx1^{gfp}$ allele responds to IFN stimulation as expected.

To confirm that $Mx1^{gfp}$ functioned as a reporter specifically for IFN signaling, we crossed the reporter line to mice deficient in IFNAR1 (type I IFN signaling deficient) or STAT2 (type I and type III IFN signaling deficient) and measured expression of GFP in the spleen after i.v. injection of PIC. GFP expression was completely lost in spleen cells from $Mx1^{gfp}/Ifnar1^{-/-}$ and in $Mx1^{gfp}/Stat2^{-/-}$ mice (Figures 1A and 1B), indicating that the reporter is specific for IFN signaling and that hematopoietic cell responses are completely dependent on type I IFN. The type I IFN receptor is thought to be expressed in all tissues and organs; however, expression of the type III IFN receptor is more restricted and thought to be mainly in epithelial cells (Pott et al., 2011; Sommereyns et al., 2008). To test the functionality of the reporter in response to type III IFN, we intranasally (i.n.) injected $Mx1^{gfp}$, $Mx1^{gfp}/Ifnar1^{-/-}$, and $Mx1^{gfp}/Stat2^{-/-}$ mice with PIC and examined GFP expression in the lung. As expected, $CD45^{+}$ hematopoietic cell GFP expression was completely dependent on IFNAR1. Additionally, $CD45^{-}CD31^{+}$ endothelial cell GFP expression was also completely dependent on IFNAR1. While $EpCAM^{+}$ epithelial cell GFP expression was largely dependent on IFNAR1, some expression was still present in $Mx1^{gfp}/Ifnar1^{-/-}$ mice. This was completely abolished in $Mx1^{gfp}/Stat2^{-/-}$ mice, confirming that the reporter functions in response to both type I and type III IFN signaling and that both pathways are important in epithelial cells (Figures 1C and 1D). While this confirms reporter functionality for both type I and type III IFN signaling, the relative importance of the pathways for the IFN response is likely to change under different conditions. It should also be noted that other cytokines have been reported to activate STAT2; therefore, while loss of GFP expression in $Stat2^{-/-}$ mice is consistent with IFN-dependence, we cannot completely exclude effects of other cytokines.

Constitutive IFN Signaling in Tissues and Monocytes

Type I IFNs are produced at low levels in the absence of infection and exert effects on a diverse array of biological processes. This is thought to occur through modulating the expression of signaling intermediates required for IFN and other cytokine responses, thus priming responses to other cytokines (Gough et al., 2012). In order to characterize the basal response to IFN *in vivo*, we first used untreated $Mx1^{gfp}$ mice as an indicator of constitutive IFN signaling in the absence of stimulation or infection. We observed GFP expression in all

tissues examined–levels were low (2%–4%) in lymph nodes and spleen, in-termediate in the lung (6%)and highest in the bone marrow (9%, Figure S2). A GFP signal was detectable in all cell types examined in the spleen and bone marrow (Figures 2A and 2B). However, Ly6C^{hi} monocytes (Ly6C^{hi}CD11b^{+}Ly6G^{-}) universally expressed high levels of GFP. We confirmed that basal GFP expression in Ly6C^{hi} monocytes was due to IFN signaling; GFP expression was completely lost in the bone marrow and spleen of *Mx1^{gfp}/Ifnar1$^{-/-}$* and *Mx1^{gfp}/Stat2$^{-/-}$* mice (Figures 2C and 2D), indicating that basal IFN responses in Ly6C^{hi} monocytes are dependent on type I IFN signaling.

We next determined if other ISGs were upregulated in Ly6C^{hi} monocytes, by sorting Ly6C^{hi} and Ly6C^{lo} monocytes from the spleens of *Mx1^{gfp}* and *Mx1^{gfp}/Stat2$^{-/-}$* mice and examining gene expression. We observed a number of other ISGs, including *Ccl2, Irf7, Oas1, Ifit2*, and *Stat2*, upregulated in Ly6C^{hi} monocytes from *Mx1^{gfp}* mice relative to Ly6C^{lo} monocytes or Ly6C^{hi} monocytes from *Mx1^{gfp}/Stat2$^{-/-}$* mice (Figure 2E). The lack of ISG induction in Ly6C^{hi} monocytes is in agreement with previous work showing a lack of ISG induction in this subset in *Ifnar$^{-/-}$* mice (Lin et al., 2014; Seo et al., 2011). We also examined signaling intermediates that could be responsible for the elevated response of Ly6C^{hi} monocytes to basal levels of IFN. No differences in the expression of *Ifnar1, Ifnar2, Stat1*, or *Irf9* were evident between Ly6C^{hi} and Ly6C^{lo} subsets; however, Ly6C^{hi} monocytes expressed higher levels of *Stat2* relative to Ly6C^{lo} monocytes (Figure 2E). The data support that Ly6C^{hi} monocytes display an IFN signaling signature; however, the underlying molecular mechanism requires further investigation.

PIC Induces a Systemic IFN Response

We next examined the interferon response in *Mx1^{gfp}* mice following systemic exposure to IFN, R848, or PIC. All of the stimuli induced an IFN response in the spleen at day 1 post-exposure (Figure S3A). This response is likely to be dose dependent; however, because PIC induced the highest response, we chose to characterize this response further. Following exposure to i.v. PIC, we observed high levels of GFP in the spleen at day 1 post-exposure, which gradually fell back to baseline by day 5 (Figures 3A and 3B). GFP expression was first detectable at approximately 4 hr post-exposure in the spleen following i.v. PIC treatment (Figure 3C). GFP expression was found in all cell types examined in the spleen; relatively low levels were induced in Ly6C^{+}CD11b^{+}LyCG^{+} neutrophils, and high levels were found in Ly6C^{hi} monocytes (Figures 3D and E). We also observed strong GFP expression in the bone marrow, spleen, lymph nodes, and lung (Figures 3F and 3G, top). In order to assess the role of route of exposure on interferon responses, we injected *Mx1^{gfp}* mice intranasally with PIC and examined GFP expression in organs. Intranasal exposure induced responses in all organs; however, they were lower in terms of percentage of GFP^{+} cells and mean fluorescence intensity (MFI) compared to systemic exposure, with the exception of the lung, which showed very high GFP expression in response to intranasal treatment (Figures 3F and 3G, bottom). Following intranasal exposure, responses in the lung remained high from day 1–4 post-exposure, whereas they peaked at day 1 in other organs (Figure S3B). This may reflect persistence of the PIC stimulus in the lung environment.Similar to systemic exposure, intranasal exposure also lead to GFP expression in a variety of cell types in the lung and again a prominent population of Ly6C^{hi}GFP^{hi}

monocytes (Figure S3C). Overall the data indicate that exposure to PIC either systemically or intranasally results in IFN responses with a clear peak that resolve within approximately 5 days and efficiently reach organs distant from the site of the stimulus.

The IFN Response to Influenza Virus Is Confined to the Lung and Draining Lymph Node

Pathogen-associated molecular patterns (PAMPs) and pathogens induce similar signaling pathways, but differ in important ways. Pathogen exposure often starts with a low infectious dose of the organism, followed by a period of replication before detection by the immune system. Additionally, pathogens express antagonists that interfere with the immune response, and organisms express host factors that limit viral replication. To examine the IFN response following pathogen exposure, we followed GFP expression after infection with influenza virus. Mice were infected with 10^2 pfu of PR8, and infection was followed for 10 days. In striking contrast to PIC, mice infected with PR8 showed no GFP expression at day 1 and day 2 post-infection in the lung, with responses first becoming detectable at day 3–4 post-infection (Figure 4A). This is in agreement with previous data suggesting “stealth” replication of influenza virus prior to the initiation of innate responses (Moltedo et al., 2009), i.e., replication for ~48 hr with no sign of induction of innate immunity. GFP responses peaked between day 6 and 7 post-infection and then gradually fell in the lung. Responses in the draining lymph node also began at day 3–4 post-infection but remained high through day 10. Also in contrast to PIC, we did not detect a GFP signal above background in organs distant from the site of infection, including the bone marrow, spleen, or non-draining lymph node (Figure 4A). Thus, responses to influenza virus were both delayed relative to PIC responses and limited at the organ level to areas of active virus replication.

The PR8 strain of influenza virus serves as a model for influenza virus infection in mice but is highly mouse adapted. We therefore examined responses to a number of other influenza virus strains of varying pathogenicity. We first examined responses to the A/Viet Nam/1203/04 (H5N1) avian strain engineered to lack the multibasic cleavage site in HA (HALo). Removal of the multibasic cleavage site causes viral replication to be restricted to the lung and allows use under BSL2 conditions; however, the virus retains several other virulence markers that contribute to pathogenicity (Steel et al., 2009). Strikingly, HALo infection led to a rapid and enhanced GFP response in the lung relative to PR8 infection at the same dose. GFP expression was detected at day 2 post-infection compared to day 3–4 for PR8 and peaked and remained high from day 2 through day 7 post-infection, when animals succumbed to infection (Figure 4B). This is in agreement with the “cytokine storm” that has been reported for H5N1 viruses (Wang et al., 2016). GFP responses in the draining lymph node were evident at day 1 post-infection, before responses in the lung. We again failed to detect GFP expression in the spleen and non-draining lymph nodes; however, a small response was detected in the bone marrow (Figure 4B). We next infected mice with the Cal09 pandemic influenza virus, which is less pathogenic in mice than PR8 or H5N1 HALo viruses (Maines et al., 2009). GFP responses to Cal09 were delayed similar to PR8 (Figure 4C); however, a number of animals in the Cal09 group showed no GFP expression, which may reflect that 10^2 pfu is close to the minimal infectious dose for this virus (Maines et al., 2009). Overall the data suggest that less pathogenic strains induce a delayed IFN response

that peaks and then resolves, while more pathogenic strains induce an early IFN response that fails to resolve and remains high until the animals succumb to infection.

In order to determine if the delay in GFP expression during PR8 infection was due simply to the infectious dose, we infected mice with increasing doses of PR8. At day 3 post-infection, doses of 10^3 and 10^4 were able to induce higher levels of GFP than the 10^2 dose. However, we did not observe GFP expression at day 2 with any of the doses (Figure 4D), suggesting that early GFP expression during H5N1 infection is due to factors other than virus replication. To assess the impact of NS1 on interferon responses, we infected mice with the PR8 R38A/K41A NS1 RNA-binding mutant, expressing an NS1 protein impaired in its ability to prevent IFN induction. As expected, infection with 10^6 pfu resulted in a high GFP response starting at day 1 postinfection and continuing through day 5 (Figure 4E). However, infection with 10^2 pfu of the NS1 mutant gave no detectable response, presumably due to a very local response that quickly restricted virus replication (Figure 4E). Thus, both viral dose and NS1 expression control the kinetics of the early IFN response.

IFN Responses to Influenza Virus Are Largely Restricted to Hematopoietic Cells

We next examined the cell types expressing GFP in the lung following influenza virus infection. Mice were infected with 10^2 pfu of PR8, and lungs were stained at the peak of GFP expression at day 7 for epithelial cells ($EpCAM^+CD31^-CD45^-$), endothelial cells ($CD31^+EpCAM^-CD45^-$), and hematopoietic cells ($CD45^+$). A strong GFP signal was observed in infiltrating hematopoietic cells, and a small signal was observed in endothelial cells (Figures 5A and 5B). Surprisingly, very little GFP was detected in epithelial cells, the target cells for influenza virus replication. We were also unable to observe expression in $CD45^-$ cells at other time points post-infection (Figure S4A). This was not due to an inability of epithelial cells to respond to IFN, as treatment with PIC led to GFP expression in greater than 90% of these cells (Figure 5A). We were, however, able to detect a GFP signal in epithelial cells using a high viral inoculum (10^6) of PR8 or the R38A/K41A NS1 mutant strain (Figures 5C and 5D). This suggests that during low-dose infection, NS1 is able to limit IFN to levels that readily trigger reporter expression in hematopoietic cells but are not sufficient for detection in epithelial cells. In support of this, treatment with lower doses of PIC was able to induce responses in hematopoietic cells at concentrations where epithelial cells did not respond (Figures 5C and D). In addition, responses to PIC appeared to be induced in a more transient manner (day 1) in epithelial cells compared to the more sustained responses (day 1–5) in hematopoietic cells (Figure S4B). Thus, although epithelial cells are capable of responding to IFN after treatment with PIC, they do not have a detectable response following low-dose influenza virus infection, likely due to a lower sensitivity to IFN.

In order to more directly compare the responses of hematopoietic cells to non-hematopoietic cells, we stimulated bone-marrow-derived macrophages and mouse embryonic fibroblasts (MEFs) with type I IFN and infected with viruses. In macrophages, we observed responses to type I interferon starting at 10 U/ml and higher responses to increasing levels of IFN. However, in MEFs, we only observed responses to IFN at 1000 U/ml. During influenza virus infection, we observed GFP at higher virus MOIs in macrophages, but did not observe GFP

in MEFs. Using PR8ΔNS1 virus, we could observe GFP in MEFs; however, we again observed responses in macrophages at much lower MOIs (Figure 5E). Western blotting for viral proteins revealed robust expression of viral proteinsin MEFs but very little expression in macrophages. We saw high levels of NS1 in MEFs but only low levels in macrophages (Figure 5F), which may suggest that NS1 expression effectively limits IFN induction in virus-infected MEFs, but expression is not sufficient in macrophages to limit IFN production.

GFP^{hi} Cells during Influenza Virus Infection Are Infected Ly6C^{hi} Monocytes

We next examined the subsets of CD45^{+} cells expressing GFP following infection. We observed varying levels of GFP among infiltrating CD45^{+} cells in the lung during infection (Figures 6A and 6B). The GFP^{lo} population was composed largely of T cells, B cells, and natural killer (NK) cells (MFI 1059, 1640, and 1086, respectively). A portion of CD11c^{+}SiglecF^{+} alveolar macrophages expressed intermediate levels of GFP (MFI 4103); however, these cells have high baseline autofluorescence in the absence of GFP expression (Figures 6A and S5A). CD11c^{hi}MHCII^{hi}CD103^{+} DCs expressed intermediate levels of GFP (MFI 3936). The GFP^{hi} population was composed of Ly6C^{hi}CD11b^{+}Ly6G^{-}CD11c^{+} inflammatory monocytes (MFI 11961). These cells expressed GFP in the absence of stimulation (Figures 2A–2D), which was further upregulated upon infection (Figure S5A, inset histogram). CD11c^{hi}MHCII^{hi}CD11b^{+} DCs also expressed high levels of GFP; however, these cells are thought to migrate to the draining lymph node following infection, and inflammatory monocytes express both CD11c and MHCII following infection, making it difficult to differentiate these subsets. Therefore, similar to non-infection conditions, Ly6C^{hi} monocytes are the predominant IFN responding subset during infection. In the draining lymph node, we observed high levels of GFP expression even at late time points post-infection (Figure 4A). We examined these cell types at day 9(D9) post-infection with PR8. GFP was observed in all cell types; however, the majority of cells in the lymph node (LN) were CD4 and CD8 T cells and B cells (Figure S5B). Therefore, following influenza virus infection, Ly6C^{hi} monocytes in the lung and T and B cells in the LN show high IFN responses.

We next determined if GFP expression correlated with viral protein expression. We measured surface M2 expression during infection with PR8. A small population of CD45-EpCAM+ epithelial cells (7%) showed M2 expression but was GFP negative (Figures 6C and 6D). We observed two other prominent populations, a GFP^{lo}M2^{-} population and a GFP^{hi}M2^{+} population (Figures 6C and 6D). The GFP^{lo}M2^{-} population was mainly composed of T and B cells, while the GFP^{hi}M2^{+} population was composed of Ly6C^{hi} monocytes. This may suggest that infection contributes to high IFN responses in monocytes.

Ly6C^{hi} Monocyte Recruitment, but Not Development, Is Dependent on IFN Signaling

In order to understand the significance of high IFN responses in Ly6C^{hi} monocytes, we examined this subset under basal and infection conditions. IFNAR1 has been reported to be required for the generation of Ly6C^{hi} monocytes (Seo et al., 2011); however, we detect the presence of both the Ly6C^{hi} inflammatory monocyte and Ly6C^{lo} patrolling monocyte populations, defined as Ly6C^{hi}CD11b^{+}Ly6G^{-} and Ly6C^{lo}CD11b^{+}Ly6G^{-}, in uninfected *Mx1^{gfp}/Stat2$^{-/-}$*(Figure 7A) mice and *Mx1^{gfp}/Ifnar1$^{-/-}$* mice (data not shown), which is in

agreement with another report (Lee et al., 2008). Ly6C is an ISG (Dumont and Coker, 1986; Lee et al., 2008) and therefore is upregulated in WT mice, but not mice deficientin IFN signaling, under infection conditions (Figure 7A). Seo et al. (2011) defined this population on the basis of Ly6C and Ly6G staining only, which includes other Ly6C expressing cells, and gated on the Ly6C^{hi} population under infection conditions, which likely explains the discrepancy.

Although *Mx1*^{gfp}/*Stat2*$^{-/-}$ mice have Ly6C^{hi} monocytes, their recruitment to the lung during influenza virus infection is severely reduced in terms of absolute numbers, with a concomitant increase in neutrophil numbers (Figure 7B), in agreement with previous findings in *Ifnar*$^{-/-}$ mice (Seo et al., 2011). We were unable to detect consistent viral titers at day 2 post-infection; however, by day 3 post-infection, *Mx1*^{gfp}/*Stat2*$^{-/-}$ mice showed slightly higher viral titers (Figure 7C), indicating that decreased recruitment of Ly6C^{hi} monocytes to the lung in *Mx1*^{gfp}/*Stat2*$^{-/-}$ mice was not due to reduced viral replication. In agreement with previous findings (Davidson et al., 2014; Lin et al., 2014; Seo et al., 2011), we find very little induction of the monocyte chemoattractants *Ccl2* and *Ccl7* in the absence of STAT2 (Figure 7D), likely because they are ISGs (Bauer et al., 2006; Rauch et al., 2013) and cannot be induced in the absence of IFN signaling. We also find no induction of *Ifnb1* (Figure 7D). These data suggest that IFN signaling is required for recruitment, but not generation, of Ly6C^{hi} monocytes; however, it is unclear if the role of IFN is direct or simply a consequence of the lack of ISG induction.

DISCUSSION

A number of reporter mouse strains have helped to define the cell types that produce IFN *in vivo* following infection; however, less is known about the dynamics of the subsequent antiviral state that is induced. Here we report the development of a reporter mouse strain that can be used to track IFN responses at the single-cell level. We show that the reporter responds to both type I and type III IFN. Importantly, reporter expression is completely lost in the absence of IFNAR, in some cell types, or STAT2, in all cell types examined. This confirms specificity of the reporter for IFN signaling, although in the case of STAT2 we cannot completely exclude that other cytokines may contribute to STAT2-mediated reporter gene expression. This model will be useful for understanding the basic biology of the type I IFN system, including the different roles of the IFN subtypes, as well as the IFN response under pathological conditions including acute and persistent infections and systemic and organ-specific autoimmunity.

A similar mouse model expressing luciferase under the control of the Mx2 promoter in the context of a BAC transgenic was previously reported (Pulverer et al., 2010). The Mx1 and Mx2 loci are thought to be regulated by IFN in a similar manner (Asano et al., 2003; Haller and Kochs, 2011; Mordstein et al., 2010). The luciferase reporter is optimal for whole body *in vivo* imaging, while GFP is more suited to single-cell studies. Following luciferase expression by *in vivo* imaging, a strong IFN response was observed in the liver. While direct comparison between the studies is difficult due to different experimental conditions and techniques for measuring the reporters, we observed longer kinetics for the IFN response to PIC, as follows: 4 days in the spleen compared to 2 days in the liver. This may reflect organ-

specific differences, different sensitivities or half-lives of the reporters, or different sensitivities of *in vivo* imaging compared to flow cytometry. In response to PIC, we found IFN responses in every organ examined, while the *in vivo* imaging study found IFN responses focused on the liver. When individual organs were isolated following treatment with IFN-β, luciferase expression was observed in other organs. Therefore, the strong signal in the liver likely masked the signal in other organs during influenza virus infection.

In response to influenza virus infection, we found that the IFN response was delayed, locally confined, and restricted in terms of cell types compared to responses to PIC. While PIC led to a high IFN response within 4 hr of treatment, we could not detect an IFN response to influenza virus until 3–4 days post-infection. This delay in the IFN response is in agreement with previous studies describing stealth replication of influenza virus for ~48 hr before detection (Moltedo et al., 2009). The kinetics of the response are in agreement with the kinetics of IFN-β expression observed in IFN-β luciferase mice (Lienenklaus et al., 2009) and Mx1 expression as measured by qPCR (Moltedo et al., 2009). In response to PR8 infection, IFN responses peaked and then began to resolve; however, in response to HALo infection, IFN responses remained at peak levels from day 2 through 5, when the animals succumbed to infection, which is in agreement with the cytokine storm that has been described for H5N1 viruses (Tisoncik et al., 2012).

We found that IFN responses to influenza virus were confined to the lung and draining LN, which are areas of active viral replication (Moltedo et al., 2011). This is in agreement with IFN-β localization to the lung in influenza-infected IFN-β luciferase mice (Lienenklaus et al., 2009). IFN produced during SeV or PR8 infection has been reported to “instruct” cells in the bone marrow into an antiviral state, before they are recruited to the lung. While both SeV and PR8 were able to induce ISG expression in the bone marrow as measured by qPCR, the fold induction was low for influenza virus. Functional experiments confirmed that SeV could induce an antiviral state in bone marrow cells; however, these experiments were not reported for influenza virus (Hermesh et al., 2010). It is possible that different strains and doses of influenza virus may be capable of inducing a more systemic response, as was suggested by a slight increase in GFP expression in the bone marrow following HALo infection.

Here we report that GFP-detectable IFN responses are restricted to a limited set of cell types in the lung following influenza virus infection. We could not detect an IFN response in epithelial cells during low-dose influenza virus infection. This was surprising given that IFN responses can readily be detected in epithelial cell lines infected *in vitro*. However, it is in agreement with a lack of reporter expression in epithelial cells following infection with WT strains of influenza virus in IFN-β luciferase mice (Kallfass et al., 2013). In bone marrow chimeras expressing a functional Mx1 protein in either the hematopoietic or non-hematopoietic compartment, protection from lethal influenza virus infection is mediated by non-hematopoietic cells (Haller et al., 1979; unpublished data). This suggests that IFN responses are functional in non-hematopoietic cells *in vivo* and that the lack of detection in our model represents a limit of detection, induction limited to a narrow anatomical region or time frame, or induction by ISRE-independent IFN pathways that would not be detected by our reporter. Higher viral inoculums or NS1-deficient strains were able to induce measurable

IFN responses in epithelial cells, in agreement with expression of Mx1 protein in epithelial cells following infection of an Mx1-sufficient strain with an NS1-deficient virus (Mordstein et al., 2010). Interestingly, the cell types producing IFN-β in response to La Crosse virus infection also change in the presence or absence of the IFN antagonist protein (Kallfass et al., 2012), suggesting that at least some viral IFN antagonists restrict the induction of IFN and ISGs in specific cell types.

We found surprisingly high IFN responses both basally and during infection in inflammatory monocytes. Monocytes are hematopoietic cells that originate from myeloid progenitors in the bone marrow and traffic to peripheral tissues via the bloodstream. They are divided into two subsets termed “inflammatory” and “patrolling” monocytes. In response to inflammatory stimuli, Ly6C^{hi} monocytes are recruited to the site of infection and differentiate into monocyte-derived cells (MCs) with different functional properties and marker expression (Duan et al., 2017; Guilliams et al., 2014; Segura and Amigorena, 2013; Xiong and Pamer, 2015). The reason for the high IFN responses in inflammatory monocytes is unknown; however, we did find that they expressed high levels of surface M2, indicating that they were infected. Monocyte infection has been reported in a few other studies (Lin et al., 2014; Pang et al., 2013). Inflammatory monocytes have also been reported to produce IFN (Lin et al., 2014) and to mediate tissue damage in mouse strains that produce high levels of IFN (Davidson et al., 2014). The basal responses we observed in inflammatory monocytes were dependent on IFN signaling, which could suggest that this subset produces low-level IFN that primes subsequent responses to infection. We did not observe differences in receptor expression or signaling components of the IFN pathway between inflammatory and patrolling monocytes, with the exception of STAT2. Whether STAT2 or other factors contribute to the high basal and induced IFN responses in inflammatory monocytes is under further investigation. We find that IFN signaling is not required for the development of inflammatory monocytes; however, it is required for their recruitment during infection. Because Ly6C is an ISG, the population defined as Ly6C^{hi} in the previous study (Seo et al., 2011) was likely a MC that had upregulated Ly6C expression under inflammatory conditions. We find that IFN signaling is required for recruitment of inflammatory monocytes during infection; whether this is a direct effect or an indirect result of the lack of chemokine induction is under further investigation.

STAR★METHODS

CONTACT FOR REAGENT AND RESOURCE SHARING

Further information and requests for resources and reagents should be directed to and will be fulfilled by the Lead Contact, Adolfo Garcia-Sastre (Adolfo.Garcia-Sastre@mssm.edu).

EXPERIMENTAL MODEL AND SUBJECT DETAILS

Animal models—6-8 week old age and sex matched mice were used for all experiments. Both males and females were used; obvious sex difference were not noted. C57BL/6J mice (Jackson) were used to set GFP gates. *Ifnar1*(Müller et al., 1994) and *Stat2*$^{-/-}$ (Park et al., 2000) mice on the C57BL/6J background have been previously described. *Ifnb*^{mob} mice on the C57BL/6J background were purchased from Jackson. Animal studies were approved by

the Institutional Animal Care and Use Committee of Icahn School of Medicine at Mount Sinai. Mice were housed in a barrier facility at the Icahn School of Medicine at Mount Sinai under specific pathogen free conditions in individually ventilated cages and feed irradiated food and filtered water.

Primary cell cultures—Bone marrow-derived macrophages were obtained by extracting bone marrow from femurs and tibias of mice, RBCs were lysed and cells were cultured for 7 days in RPMI 1640 (GIBCO) containing 10% FBS (Hyclone), Penicillin, Streptomycin, L-glutamine, HEPES (Cellgro), β-ME, and 10 ng/ml rmM-CSF (R&D Systems). Macrophages were removed from the plate following incubation with cold PBS and plated in 12-well plates at 1×10^5/well. P2 MEFs were trypsinized and plated similarly. Cells were cultured at 37°C in 5% CO_2.

METHOD DETAILS

Generation of Mx1^{gfp} mice—The *Mx^{gfp}* targeting vector was constructed using the recombineering protocol described in Wu et al. (2008). Briefly, a portion of the C57BL/6J BAC clone RP24-363P1 (BACPAC) was transferred into pACYC177 (NEB), and an AscI restriction site was inserted into exon 2 of Mx1 at the natural translation start site using red recombinase. A fusion protein of maxGFP-GSGGS-OVA(229-358) and the ACN cassette containing a self-excising neomycin (Wu et al., 2008) was inserted into the AscI site, and DTx cloned out of PGKneolox2DTA (Soriano, 1997) was inserted into the plasmid backbone. The targeting vector was electroporated into C57BL6 Bruce4 ES cells at the Transgenic Mouse Core at Harvard Medical School and injected into BALB/c blastocysts at the Mouse Genetics and Gene Targeting CoRE at Icahn School of Medicine at Mt. Sinai. Germline transmission was confirmed by Southern blot and PCR. Southern blotting was performed by alkaline transfer, digesting DNA with AseI and probing with PCR product generated with primers the primers listed in Table S1. Mice were genotyped with GoTaq Flexi DNA polymerase (Promega) the primers WT-F, WT-R, and KI-R listed in Table S1 and PCR conditions: 94°C 30 s, 55°C 30 s, 72°C 30 s.

Organ isolations—Bone marrow was flushed from femurs and tibias, spleen and LNs were mechanically disrupted with the plunger of a syringe, and lungs were digested for 40 min in 1 mg/ml collagenase type 4 (Worthington) 5% FBS in DMEM. Cells were then filtered through a 0.2 μm cell strainer and RBCs were lysed. For experiments staining lung epithelial cells, an alternative protocol was used to obtain viable epithelial cells – mice were perfused with PBS through the right ventricle and then instilled intratracheally with 2 mL 50 U/ml dispase (BD) in HBSS and 500 μL 1% LMA agarose (Lonza) warmed to 45°C. Lungs were covered with ice for 2 min, removed to a tube containing 2 mL dispase, and incubated at RT for 45 min. Tissue was disintegrated with forceps in 95 KU/ml DNase I (Sigma) in DMEM and incubated for 10 min at RT. Cells were then filtered and any remaining RBCs were lysed.

Flow cytometry and cell sorting—Cells were suspended in 3% FBS 2mM EDTA in PBS and staining was performed in the presence of 2% NRS, 2% Fc block (BD), and fixable viability dye eFluor 450 (eBioscience). Cells were stained with the following antibodies

from BD: CD3-APC (145-2C11), CD19- APC (1D3), CD11c-V450 or PE-Cy7 (HL3), NK1.1-APC (PK136), Ly6G-V450 (1A8), Ly6C-PerCP-Cy5.5 (AL-21), CD11b-PE (M1/70), B220-APC (RA3-6B2), CD45-APC (30-F11), SiglecF-BV421 (E50-2440), CD8-PerCP-Cy5.5 (53-6.7). And the following antibodies from eBioscience: CD103-APC (2E7), EpCAM-PE-Cy7 (G8.8), CD31-PerCP-eFluor 710 (390), MHC Class II (I-A/I-E) eFluor 450 (M5/114.15.2), FasL-APC (MFL3), CD4-APC (GK1.5), and from R&D: CCR2-APC (475301). Alexa Fluor 647 protein labeling kit (Thermo) was used to label the influenza M2 (E10) (Bourmakina and García-Sastre, 2005) antibody. Cells were fixed with 2% formaldehyde after staining and analyzed on an LSRII after gating for FSC/SSC, singlets, and live cells. Cells were quantitated by flow cytometry with AccuCount Particles (Spherotech). Sorting was performed similarly on FACSAria.

Infections and TLR stimulation—Mice were injected with 50 or 100 μg Poly(I:C) HMW (Invivogen), 15,000 U universal type I IFN (PBL Interferon), or 35 ug R848 (Invivogen) in PBS (in 50 μL for i.n. or 200 μL for i.v.). Mice were infected with the following viruses at the doses indicated in 20 μL PBS: A/PR/8/34 (H1N1) (PR8), A/Viet Nam/1203/04 (H5N1) lacking the multibasic cleavage site (HALo) (Steel et al., 2009), A/California/04/09 (H1N1) (Cal09) (Hai et al., 2010), A/PR/8/34 (H1N1) delNS1 (García-Sastre et al., 1998b) (delNS1), A/PR/8/34 (H1N1) NS1 R38A/K41A (Talon et al., 2000) (PR8 NS1 R38A/K41A). Viral titer was determined by plaque assay on MDCK cells. Macrophages and MEFs were stimulated with universal type I IFN (PBL Interferon) or infected with virus. The following day cells were stained with eFluor 455UV viability dye (eBioscience) and fixed with 4% PFA for flow cytometry.

Western blots—For western blots, 2×10^5 macrophages or MEFs were plated in 12-well plates and infected at the indicated MOI, lysed in RIPA buffer containing Halt Protease and Phosphatase Inhibitor Cocktail (Thermo), denatured in Laemmli buffer, run on 4%-12% Bis-Tris gels (Thermo), and transferred to PVDF membranes. Membranes were blocked with 5% nonfat milk 0.1% Tween-20 in PBS and probed with mouse anti-NP (HT-103), (Kerafast) rabbit polyclonal anti-NS1 (1-73) (Solórzano et al., 2005), and rabbit β-Actin mAb HRP Conjugate (Cell Signaling).

qRT-PCR—Total RNA was extracted from sorted spleen cells or collagenase-digested lung using using EZNA total RNA kit and RNase-free DNase (Omega). RNA was reverse-transcribed using Maxima Reverse Transcriptase and oligo-dT (Thermo). Quantitative RT-PCR was performed on cDNA using LightCycler 480 SYBR Green I Master Mix (Roche) and the primers listed in Table S1 on a LightCycler 480 II.

QUANTIFICATION AND STATISTICAL ANALYSIS

Graphpad Prism 7.0 was used to calculate significance using unpaired t test. Statistical details are indicated in the figure legends.

Supplementary Material

Refer to Web version on PubMed Central for supplementary material.

ACKNOWLEDGMENTS

We thank the Mouse Genetics and Gene Targeting CoRE at Icahn School of Medicine at Mount Sinai for their assistance with the production of the mice used for this study and Christian Schindler for originally providing the *Stat2*$^{-/-}$ mice.We are grateful to Richard Cadagan and Osman Lizardo for excellent technical assistance. This work was partially supported by the Center for Research on Influenza Pathogenesis, an NIAID funded Center of Excellence for Influenza Research and Surveillance (CEIRS, contract HHSN272201400008C to A.G.-S. and M.B.U.).

REFERENCES

Asano A, Jin HK, and Watanabe T (2003). Mouse Mx2 gene: organization, mRNA expression and the role of the interferon-response promoter in its regulation. Gene 306, 105–113. [PubMed: 12657472]

Barbalat R, Lau L, Locksley RM, and Barton GM (2009). Toll-like receptor 2 on inflammatory monocytes induces type I interferon in response to viral but not bacterial ligands. Nat. Immunol. 10, 1200–1207. [PubMed: 19801985]

Bauer JW, Baechler EC, Petri M, Batliwalla FM, Crawford D, Ortmann WA, Espe KJ, Li W, Patel DD, Gregersen PK, and Behrens TW (2006). Elevated serum levels of interferon-regulated chemokines are biomarkers for active human systemic lupus erythematosus. PLoS Med. 3, e491. [PubMed: 17177599]

Bourmakina SV, and García-Sastre A (2005). The morphology and composition of influenza A virus particles are not affected by low levels of M1 and M2 proteins in infected cells. J. Virol. 79, 7926–7932. [PubMed: 15919950]

Ciancanelli MJ, Abel L, Zhang SY, and Casanova JL (2016). Host genetics of severe influenza: from mouse Mx1 to human IRF7. Curr. Opin. Immunol. 38, 109–120. [PubMed: 26761402]

Davidson S, Crotta S, McCabe TM, and Wack A (2014). Pathogenic potential of interferon αβ in acute influenza infection. Nat. Commun. 5, 3864. [PubMed: 24844667]

Dresing P, Borkens S, Kocur M, Kropp S, and Scheu S (2010). A fluorescence reporter model defines "Tip-DCs" as the cellular source of interferon β in murine listeriosis. PLoS ONE 5, e15567. [PubMed: 21179567]

Duan M, Hibbs ML, and Chen W (2017). The contributions of lung macrophage and monocyte heterogeneity to influenza pathogenesis. Immunol. Cell Biol. 95, 225–235. [PubMed: 27670791]

Dumont FJ, and Coker LZ (1986). Interferon-alpha/beta enhances the expression of Ly-6 antigens on T cells in vivo and in vitro. Eur. J. Immunol. 16, 735–740. [PubMed: 3487457]

García-Sastre A, Durbin RK, Zheng H, Palese P, Gertner R, Levy DE, and Durbin JE (1998a). The role of interferon in influenza virus tissue tropism. J. Virol. 72, 8550–8558. [PubMed: 9765393]

García-Sastre A, Egorov A, Matassov D, Brandt S, Levy DE, Durbin JE, Palese P, and Muster T (1998b). Influenza A virus lacking the NS1 gene replicates in interferon-deficient systems. Virology 252, 324–330. [PubMed: 9878611]

Goritzka M, Makris S, Kausar F, Durant LR, Pereira C, Kumagai Y, Culley FJ, Mack M, Akira S, and Johansson C (2015). Alveolar macrophage-derived type I interferons orchestrate innate immunity to RSV through recruitment of antiviral monocytes. J. Exp. Med. 212, 699–714. [PubMed: 25897172]

Gough DJ, Messina NL, Clarke CJ, Johnstone RW, and Levy DE (2012). Constitutive type I interferon modulates homeostatic balance through tonic signaling. Immunity 36, 166–174. [PubMed: 22365663]

Guilliams M, Ginhoux F, Jakubzick C, Naik SH, Onai N, Schraml BU, Segura E, Tussiwand R, and Yona S (2014). Dendritic cells, monocytes and macrophages: a unified nomenclature based on ontogeny. Nat. Rev. Immunol. 14, 571–578. [PubMed: 25033907]

Hai R, Schmolke M, Varga ZT, Manicassamy B, Wang TT, Belser JA, Pearce MB, García-Sastre A, Tumpey TM, and Palese P (2010). PB1-F2 expression by the 2009 pandemic H1N1 influenza virus has minimal impact on virulence in animal models. J. Virol. 84, 4442–4450. [PubMed: 20181699]

Haller O, and Kochs G (2011). Human MxA protein: an interferon-induced dynamin-like GTPase with broad antiviral activity. J. Interferon Cytokine Res. 31, 79–87. [PubMed: 21166595]

Haller O, Arnheiter H, and Lindenmann J (1979). Natural, genetically determined resistance toward influenza virus in hemopoietic mouse chimeras. Role of mononuclear phagocytes. J. Exp. Med. 150, 117–126. [PubMed: 36443]

Hermesh T, Moltedo B, Moran TM, and López CB (2010). Antiviral instruction of bone marrow leukocytes during respiratory viral infections. Cell Host Microbe 7, 343–353. [PubMed: 20478536]

Honda K, Yanai H, Negishi H, Asagiri M, Sato M, Mizutani T, Shimada N, Ohba Y, Takaoka A, Yoshida N, and Taniguchi T (2005). IRF-7 is the master regulator of type-I interferon-dependent immune responses. Nature 434, 772–777. [PubMed: 15800576]

Ivashkiv LB, and Donlin LT (2014). Regulation of type I interferon responses. Nat. Rev. Immunol. 14, 36–49. [PubMed: 24362405]

Jung A, Kato H, Kumagai Y, Kumar H, Kawai T, Takeuchi O, and Akira S (2008). Lymphocytoid choriomeningitis virus activates plasmacytoid dendritic cells and induces a cytotoxic T-cell response via MyD88. J. Virol. 82, 196–206. [PubMed: 17942529]

Kalejta RF, Shenk T, and Beavis AJ (1997). Use of a membrane-localized green fluorescent protein allows simultaneous identification of transfected cells and cell cycle analysis by flow cytometry. Cytometry 29, 286–291. [PubMed: 9415410]

Kallfass C, Ackerman A, Lienenklaus S, Weiss S, Heimrich B, and Staeheli P (2012). Visualizing production of beta interferon by astrocytes and microglia in brain of La Crosse virus-infected mice. J. Virol. 86, 11223–11230. [PubMed: 22875966]

Kallfass C, Lienenklaus S, Weiss S, and Staeheli P (2013). Visualizing the beta interferon response in mice during infection with influenza A viruses expressing or lacking nonstructural protein 1. J. Virol. 87, 6925–6930. [PubMed: 23576514]

Kim CC, Nelson CS, Wilson EB, Hou B, DeFranco AL, and DeRisi JL (2012). Splenic red pulp macrophages produce type I interferons as early sentinels of malaria infection but are dispensable for control. PLoS ONE 7, e48126. [PubMed: 23144737]

Kochs G, Martínez-Sobrido L, Lienenklaus S, Weiss S, García-Sastre A, and Staeheli P (2009). Strong interferon-inducing capacity of a highly virulent variant of influenza A virus strain PR8 with deletions in the NS1 gene. J. Gen. Virol. 90, 2990–2994. [PubMed: 19726611]

Kumagai Y, Takeuchi O, Kato H, Kumar H, Matsui K, Morii E, Aozasa K, Kawai T, and Akira S (2007). Alveolar macrophages are the primary interferon-alpha producer in pulmonary infection with RNA viruses. Immunity 27, 240–252. [PubMed: 17723216]

Lee PY, Weinstein JS, Nacionales DC, Scumpia PO, Li Y, Butfiloski E, van Rooijen N, Moldawer L, Satoh M, and Reeves WH (2008). A novel type I IFN-producing cell subset in murine lupus. J. Immunol. 180,5101–5108. [PubMed: 18354236]

Lienenklaus S, Cornitescu M, Zietara N, Łyszkiewicz M, Gekara N, Jabłónska J, Edenhofer F, Rajewsky K, Bruder D, Hafner M, et al. (2009). Novel reporter mouse reveals constitutive and inflammatory expression of IFN-beta in vivo. J. Immunol. 183, 3229–3236. [PubMed: 19667093]

Lin SJ, Lo M, Kuo RL, Shih SR, Ojcius DM, Lu J, Lee CK, Chen HC, Lin MY, Leu CM, et al. (2014). The pathological effects of CCR2+ inflammatory monocytes are amplified by an IFNAR1-triggered chemokine feedback loop in highly pathogenic influenza infection. J. Biomed. Sci. 21, 99. [PubMed: 25407417]

Maines TR, Jayaraman A, Belser JA, Wadford DA, Pappas C, Zeng H, Gustin KM, Pearce MB, Viswanathan K, Shriver ZH, et al. (2009). Transmission and pathogenesis of swine-origin 2009 A(H1N1) influenza viruses in ferrets and mice. Science 325, 484–487. [PubMed: 19574347]

McNab F, Mayer-Barber K, Sher A, Wack A, and O'Garra A (2015). Type I interferons in infectious disease. Nat. Rev. Immunol. 15, 87–103. [PubMed: 25614319]

Moltedo B, López CB, Pazos M, Becker MI, Hermesh T, and Moran TM (2009). Cutting edge: stealth influenza virus replication precedes the initiation of adaptive immunity. J. Immunol. 183, 3569–3573. [PubMed: 19717515]

Moltedo B, Li W, Yount JS, and Moran TM (2011). Unique type I interferon responses determine the functional fate of migratory lung dendritic cells during influenza virus infection. PLoS Pathog. 7, e1002345. [PubMed: 22072965]

Mordstein M, Kochs G, Dumoutier L, Renauld JC, Paludan SR, Klucher K, and Staeheli P (2008). Interferon-lambda contributes to innate immunity of mice against influenza A virus but not against hepatotropic viruses. PLoS Pathog. 4, e1000151. [PubMed: 18787692]

Mordstein M, Neugebauer E, Ditt V, Jessen B, Rieger T, Falcone V, Sorgeloos F, Ehl S, Mayer D, Kochs G, et al. (2010). Lambda interferon renders epithelial cells of the respiratory and gastrointestinal tracts resistant to viral infections. J. Virol. 84, 5670–5677. [PubMed: 20335250]

Müller U, Steinhoff U, Reis LF, Hemmi S, Pavlovic J, Zinkernagel RM, and Aguet M (1994). Functional role of type I and type II interferons in antiviral defense. Science 264, 1918–1921. [PubMed: 8009221]

Pang IK, Pillai PS, and Iwasaki A (2013). Efficient influenza A virus replication in the respiratory tract requires signals from TLR7 and RIG-I. Proc. Natl. Acad. Sci. USA 110, 13910–13915. [PubMed: 23918369]

Park C, Li S, Cha E, and Schindler C (2000). Immune response in Stat2 knockout mice. Immunity 13, 795–804. [PubMed: 11163195]

Pott J, Mahlakõiv T, Mordstein M, Duerr CU, Michiels T, Stockinger S, Staeheli P, and Hornef MW (2011). IFN-lambda determines the intestinal epithelial antiviral host defense. Proc. Natl. Acad. Sci. USA 108, 7944–7949. [PubMed: 21518880]

Pulverer JE, Rand U, Lienenklaus S, Kugel D, Zietara N, Kochs G, Naumann R, Weiss S, Staeheli P, Hauser H, and Köster M (2010). Temporal and spatial resolution of type I and III interferon responses in vivo. J. Virol. 84, 8626–8638. [PubMed: 20573823]

Rauch I, Müller M, and Decker T (2013). The regulation of inflammation by interferons and their STATs. JAK-STAT 2, e23820. [PubMed: 24058799]

Rodero MP, Decalf J, Bondet V, Hunt D, Rice GI, Werneke S, McGlasson SL, Alyanakian MA, Bader-Meunier B, Barnerias C, et al. (2017). Detection of interferon alpha protein reveals differential levels and cellular sources in disease. J. Exp. Med. 214, 1547–1555. [PubMed: 28420733]

Salomon R, Hoffmann E, and Webster RG (2007). Inhibition of the cytokine response does not protect against lethal H5N1 influenza infection. Proc. Natl. Acad. Sci. USA 104, 12479–12481. [PubMed: 17640882]

Scheu S, Dresing P, and Locksley RM (2008). Visualization of IFNbeta production by plasmacytoid versus conventional dendritic cells under specific stimulation conditions in vivo. Proc. Natl. Acad. Sci. USA 105, 20416–20421. [PubMed: 19088190]

Segura E, and Amigorena S (2013). Inflammatory dendritic cells in mice and humans. Trends Immunol. 34, 440–445. [PubMed: 23831267]

Seo SU, Kwon HJ, Ko HJ, Byun YH, Seong BL, Uematsu S, Akira S, and Kweon MN (2011). Type I interferon signaling regulates Ly6C(hi) monocytes and neutrophils during acute viral pneumonia in mice. PLoS Pathog. 7, e1001304. [PubMed: 21383977]

Solodova E, Jablonska J, Weiss S, and Lienenklaus S (2011). Production of IFN-β during Listeria monocytogenes infection is restricted to monocyte/macrophage lineage. PLoS ONE 6, e18543. [PubMed: 21494554]

Solórzano A, Webby RJ, Lager KM, Janke BH, García-Sastre A, and Richt JA (2005). Mutations in the NS1 protein of swine influenza virus impair anti-interferon activity and confer attenuation in pigs. J. Virol. 79, 7535–7543. [PubMed: 15919908]

Sommereyns C, Paul S, Staeheli P, and Michiels T (2008). IFN-lambda (IFN-lambda) is expressed in a tissue-dependent fashion and primarily acts on epithelial cells in vivo. PLoS Pathog. 4, e1000017. [PubMed: 18369468]

Soriano P (1997). The PDGF alpha receptor is required for neural crest cell development and for normal patterning of the somites. Development 124, 2691–2700. [PubMed: 9226440]

Staeheli P, Grob R, Meier E, Sutcliffe JG, and Haller O (1988). Influenza virus-susceptible mice carry Mx genes with a large deletion or a nonsense mutation. Mol. Cell. Biol. 8, 4518–4523. [PubMed: 2903437]

Steel J, Lowen AC, Pena L, Angel M, Solórzano A, Albrecht R, Perez DR, García-Sastre A, and Palese P (2009). Live attenuated influenza viruses containing NS1 truncations as vaccine candidates against H5N1 highly pathogenic avian influenza. J. Virol. 83, 1742–1753. [PubMed: 19073731]

Steinhauer DA (1999). Role of hemagglutinin cleavage for the pathogenicity of influenza virus. Virology 258, 1–20. [PubMed: 10329563]

Szretter KJ, Gangappa S, Belser JA, Zeng H, Chen H, Matsuoka Y, Sambhara S, Swayne DE, Tumpey TM, and Katz JM (2009). Early control of H5N1 influenza virus replication by the type I interferon response in mice. J. Virol. 83, 5825–5834. [PubMed: 19297490]

Talon J, Horvath CM, Polley R, Basler CF, Muster T, Palese P, and García-Sastre A (2000). Activation of interferon regulatory factor 3 is inhibited by the influenza A virus NS1 protein. J. Virol. 74, 7989–7996. [PubMed: 10933707]

Tisoncik JR, Korth MJ, Simmons CP, Farrar J, Martin TR, and Katze MG (2012). Into the eye of the cytokine storm. Microbiol. Mol. Biol. Rev. 76, 16–32. [PubMed: 22390970]

Wang Z, Loh L, Kedzierski L, and Kedzierska K (2016). Avian Influenza Viruses, Inflammation, and CD8(+) T Cell Immunity. Front. Immunol 7, 60. [PubMed: 26973644]

Wu S, Ying G, Wu Q, and Capecchi MR (2008). A protocol for constructing gene targeting vectors: generating knockout mice for the cadherin family and beyond. Nat. Protoc. 3, 1056–1076. [PubMed: 18546598]

Xiong H, and Pamer EG (2015). Monocytes and infection: modulator, messenger and effector. Immunobiology 220, 210–214. [PubMed: 25214476]

Highlights

- ISRE reporter mouse tracks interferon (IFN) responses *in vivo*
- IFN responses largely limited to hematopoietic cells during infection
- High basal and induced IFN responses in Ly6C^{hi} inflammatory monocytes
- Ly6C^{hi} inflammatory monocyte development not dependent on IFNs

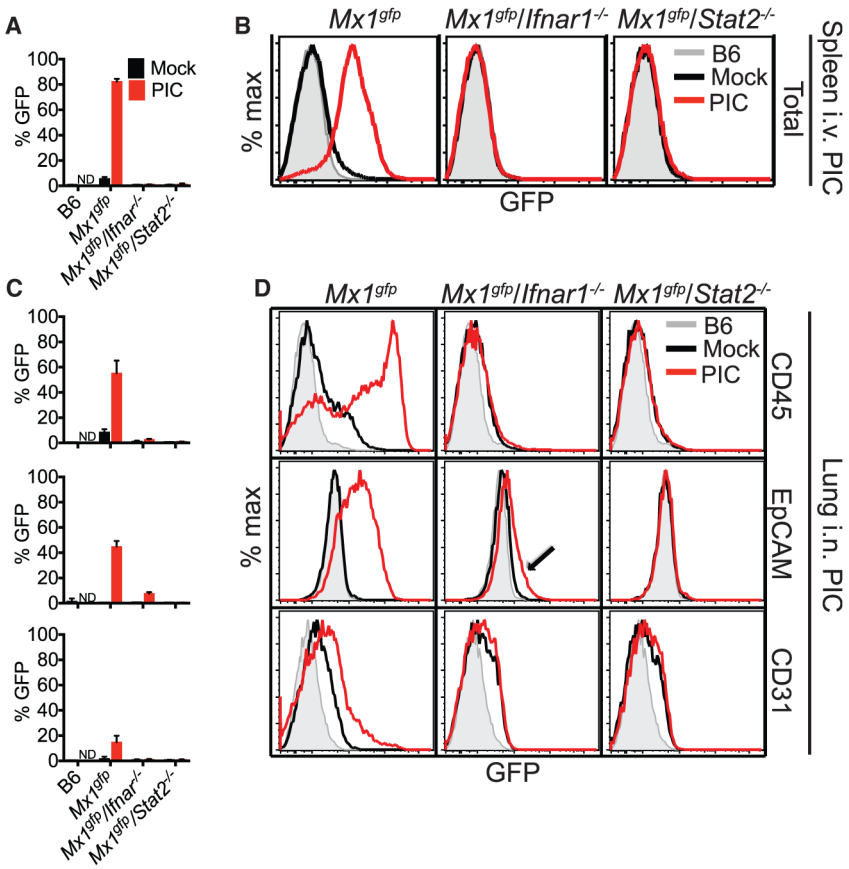

Figure 1. The *Mx1*^{gfp} Allele Functions As a Reporter for Type I and Type III IFN Responses

(A and B) *Mx1*^{gfp}, *Mx1*^{gfp}/*Ifnar1*$^{-/-}$, and *Mx1*^{gfp}/*Stat2*$^{-/-}$ mice were i.v. injected with 100 μg of PIC, and GFP expression in the spleen was measured at 24 hr.

(C and D) *Mx1*^{gfp}, *Mx1*^{gfp}/*Ifnar1*$^{-/-}$, and *Mx1*^{gfp}/ *Stat2*$^{-/-}$ mice were i.n. injected with 50 μg of PIC, and GFP expression was measured at 24 hr.

Arrow indicates IFNAR1-independent reporter expression in epithelial cells. (A) and (C) show mean ± SD for n = 3 animals. (B) and (D) show representative FACs plots. See also Figure S1.

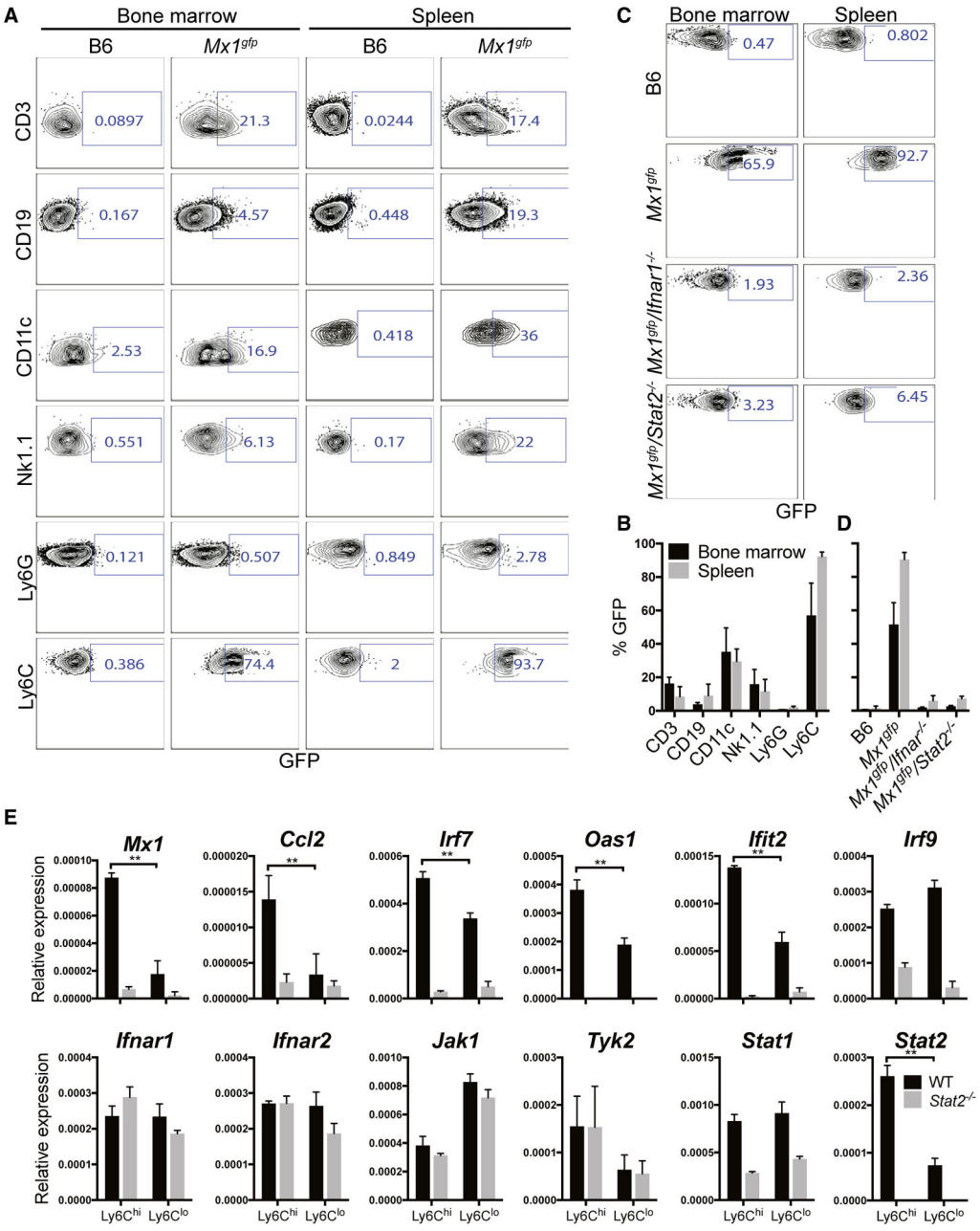

Figure 2. Basal IFN Responses Are Present at High Levels in Ly6C^{hi} Monocytes

(A and B) Bone marrow and spleen cells from untreated B6 or *Mx1^{gfp}* mice were stained for T cells (CD3$^+$), B cells (CD19$^+$), DCs (CD11c$^+$), NK cells (NK1.1$^+$), neutrophils (Ly6C$^+$Ly6G$^+$CD11b$^+$), or monocytes (Ly6C$^+$Ly6G$^-$CD11b$^+$), and GFP expression was examined.

(C and D) Bone marrow or spleen was harvested from the indicated untreated mice, and GFP expression on Ly6C^{hi}Ly6G$^-$CD11b$^+$ monocytes was analyzed.

(E) qPCR on sorted spleen Ly6C^{hi}Ly6G$^-$CD11b$^+$ and Ly6C^{lo}Ly6G$^-$CD11b$^+$ monocytes from untreated *Mx1^{gfp}* and *Mx1^{gfp}/Stat2$^{-/-}$* mice.

(B) shows mean ± SD for n = 4 animals. (D) shows mean ± SD for n = 3 animals. (E) shows mean ± SD for n = 3 animals. **indicates significance of $p < 0.01$ using unpaired t test. (A) and (C) show representative FACs plots. See also Figure S2.

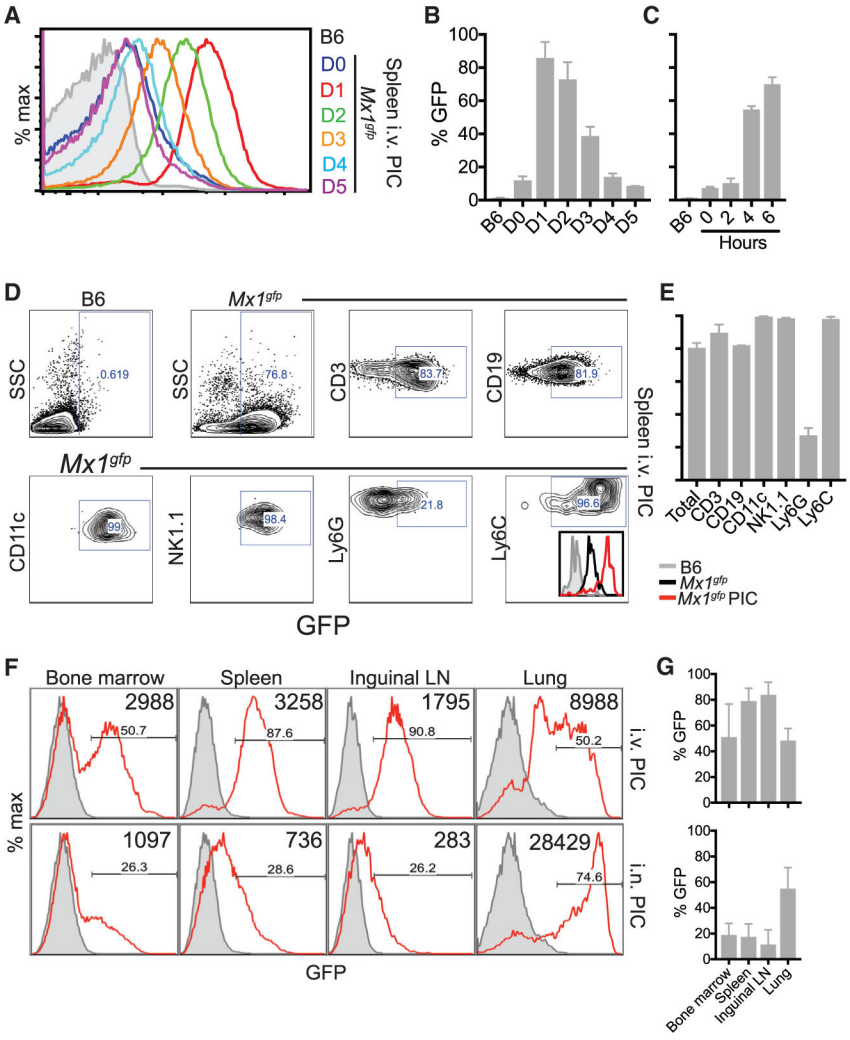

Figure 3. Exposure to PIC Induces a Systemic IFN Response

(A–C) *Mx1*^{gfp} mice were i.v. injected with 100 μg of PIC, and GFP expression in the spleen was measured at days 0–5 post-treatment (A and B) or 2, 4, or 6 hr post-treatment (C).

(D and E) *Mx1*^{gfp} mice were i.v. injected with 100 μg of PIC, and GFP expression was measured in T cells (CD3^{+}), B cells (CD19^{+}), DCs (CD11c^{+}), NK cells (NK1.1^{+}), neutrophils (Ly6C^{+}Ly6G^{+}CD11b^{+}), and monocytes (Ly6C^{+}Ly6G^{-}CD11b^{+}) in the spleen at 24 hr. Inset histogram shows basal and induced GFP expression in Ly6C^{hi} monocytes.

(F and G) *Mx1*^{gfp} mice were i.v. or i.n. injected with 50 μg of PIC, and GFP expression in organs was measured at 24 hr.

(B), (C), (E), and (G) show mean ± SD for n = 2–3 animals. (A), (D), and (F) show representative FACs plots. See also Figure S3.

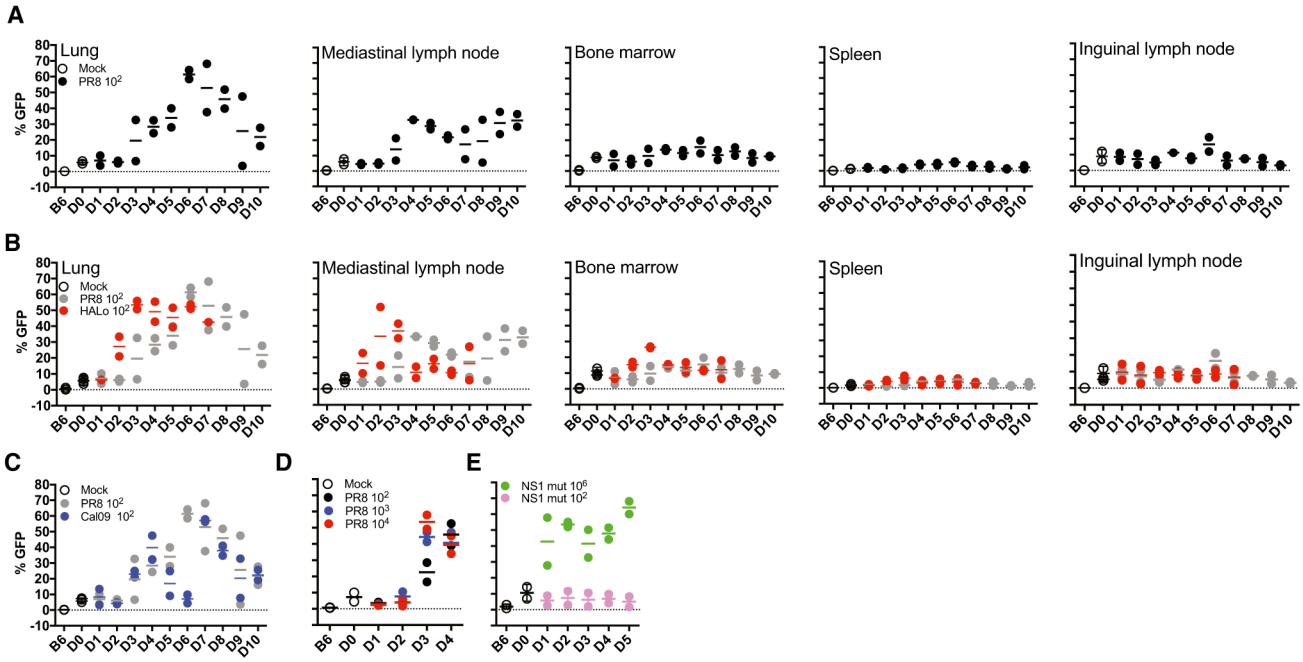

Figure 4. The IFN Response to Influenza Virus Is Confined to the Lung and Draining Lymph Node

(A and B) *Mx1*^{gfp} mice were infected with 10^2 pfu of PR8 (A) or HALo (B), and GFP expression in organs was examined at days 0–10 post-infection.

(C) *Mx1*^{gfp} mice were infected with 10^2 pfu of Cal09, and GFP expression in the lungs was examined.

(D) *Mx1*^{gfp} mice were infected with increasing doses of PR8, and GFP expression was measured in the lung.

(E) *Mx1*^{gfp} mice were infected with PR8 or the PR8-NS1 RNA-binding mutant virus (R38A/K41A), and GFP expression was measured in the lung. The bar represents the mean for n = 2 animals for all panels. Data from (A) are shown shaded in (B) and (C) for comparison.

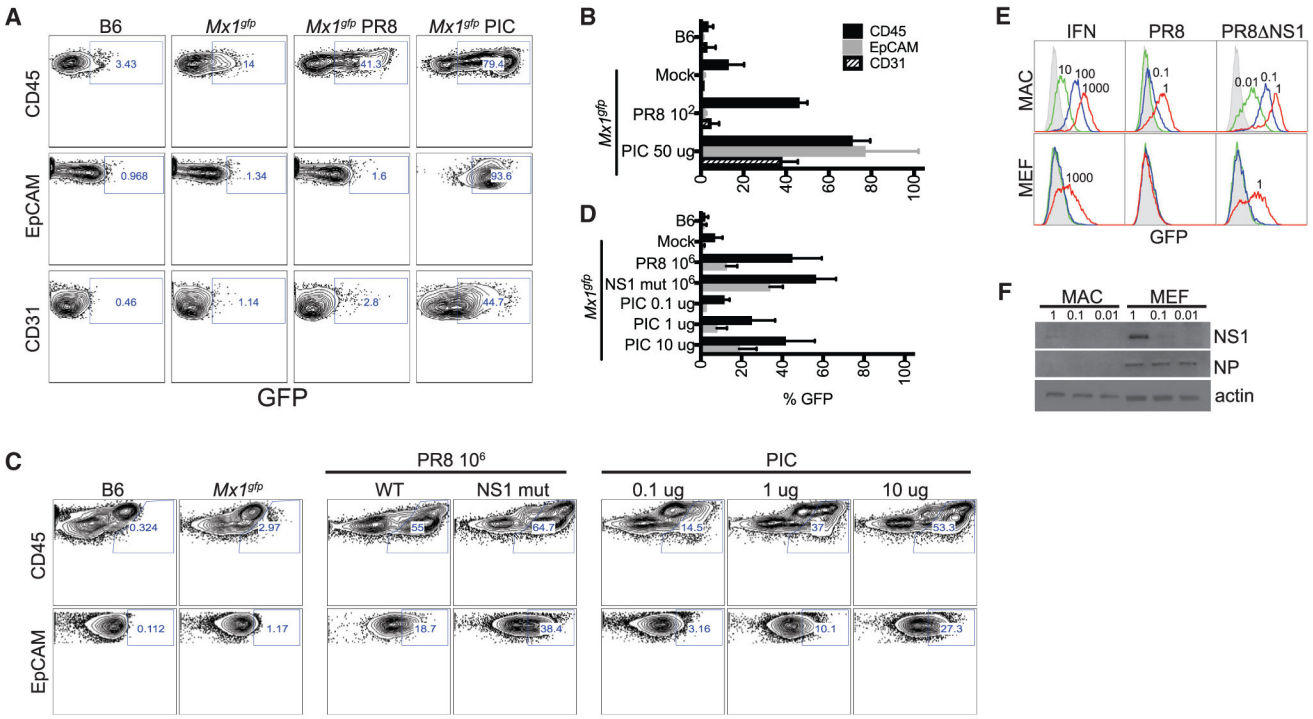

Figure 5. The IFN Response to Influenza Virus Is Largely Restricted to Hematopoietic Cells in the Lung

(A and B) *Mx1^gfp* mice were stained for hematopoietic cells (CD45+), epithelial cells (EpCAM+CD45−), or endothelial cells (CD31+) in the lung at day 7 post-infection with 10^2 pfu of PR8 or at day 1 post-treatment with 50 μg of i.n. PIC.

(C and D) *Mx1^gfp* mice were infected with 10^6 pfu of PR8 or PR8-NS1 R38A/K41A or treated i.n. with the indicated amount of PIC, and GFP expression was measured in hematopoietic and epithelial cells at day 1.

(E and F) Macrophages and MEFs were stimulated with universal type I IFN or infected with PR8 or PR8ΔNS1 at different MOIs, and GFP was measured (E) or viral gene expression was determined (F) at 24 hr post-infection.

(B) and (D) show the mean ± SD for n = 3 animals. (A), (C), and (E) show representative FACs plots. See also Figure S4.

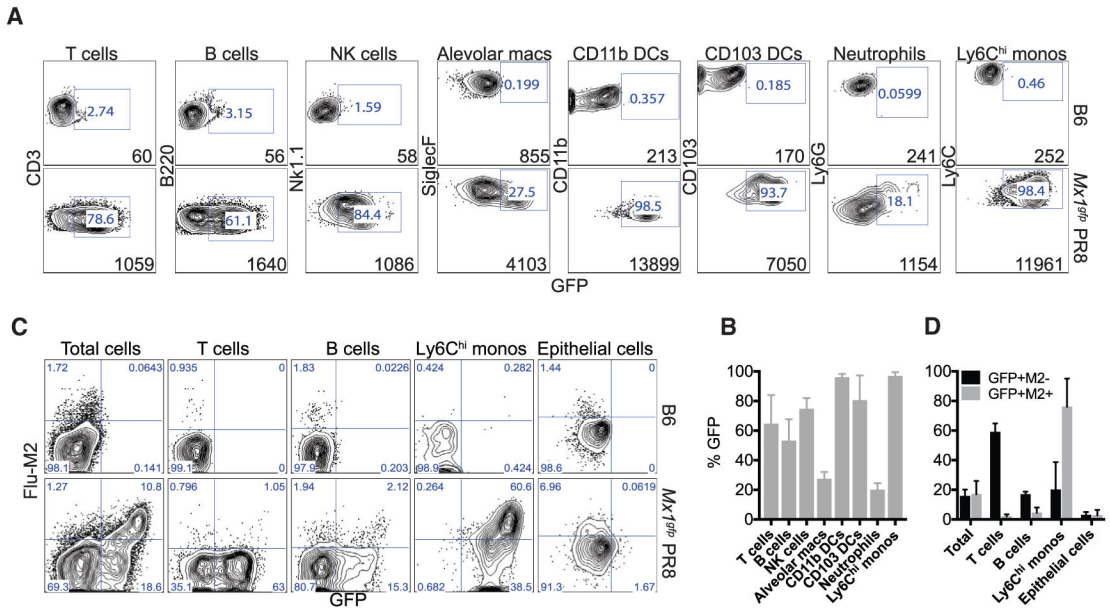

Figure 6. GFP^{hi} Cells during Influenza Virus Infection Are Infected Ly6C^{hi} Monocytes

(A and B) *Mx1^{gfp}* mice were infected with 10^2 pfu of PR8, and GFP expression was measured in T cells (CD3$^+$), B cells (B220$^+$), NK cells (NK1.1 $^+$), alveolar macrophages (CD11c$^+$SiglecF$^+$), CD11b DCs (CD11c^{hi}MHCII^{hi}CD11b$^+$CD103$^-$), CD103 DCs (CD11c^{hi}MHCII^{hi}CD103$^+$CD11b$^-$), neutrophils (Ly6C$^+$Ly6G$^+$CD11b$^+$), and Ly6C^{hi} monocytes (Ly6C^{hi}Ly6G$^-$CD11b$^+$) at day 7 post-infection.

(C and D) *Mx1^{gfp}* mice were infected with 10^4 pfu of PR8 and stained for surface M2 protein in T cells, B cells, Ly6C^{hi} monocytes, or epithelial cells at day 3.

(B) shows the mean ± SD for n = 4–6 animals. (D) shows the mean ± SD for 3 animals. (A) and (C) show representative FACs plots. See also Figure S5.

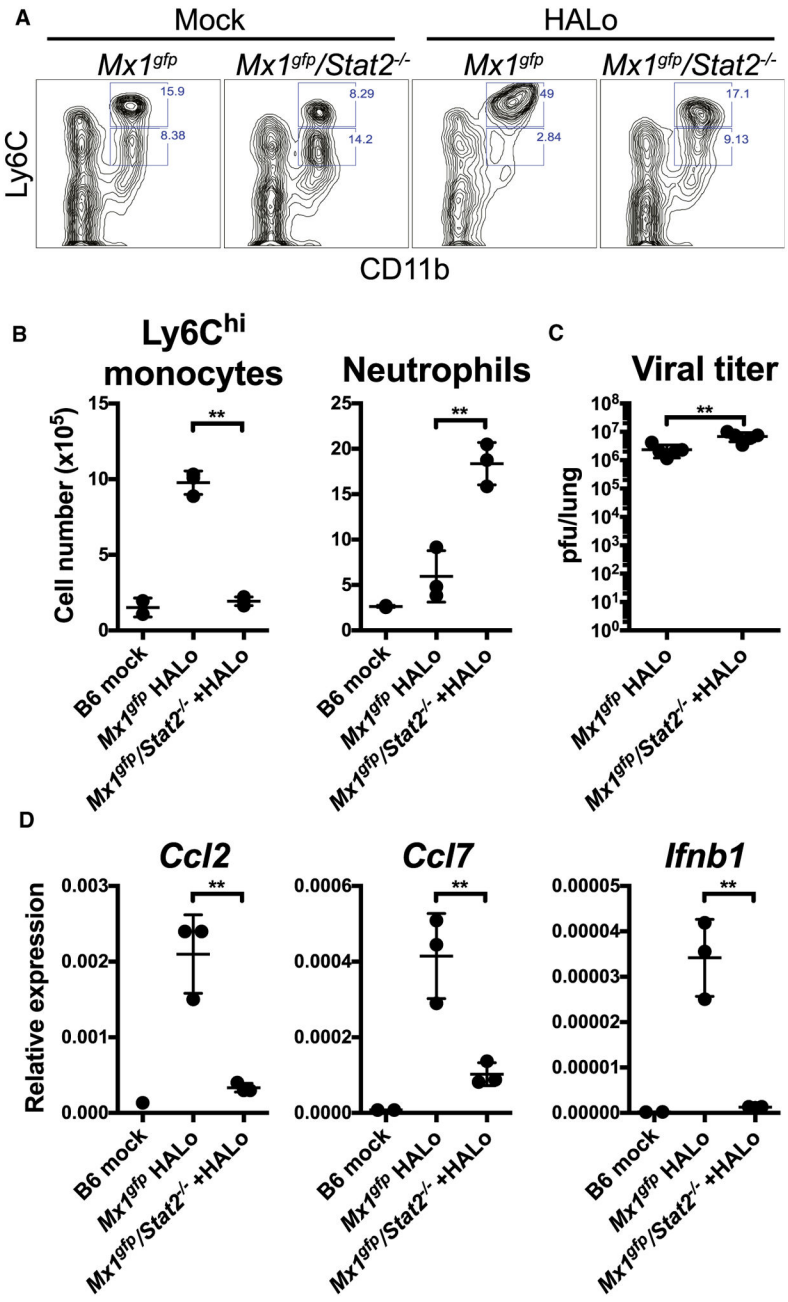

Figure 7. Ly6C^{hi} Monocyte Recruitment, but Not Development, Is Dependent on IFN Signaling

(A) *Mx1*^{gfp} and *Mx1*^{gfp}/*Stat2*$^{-/-}$ mice were mock infected or infected with 10^2 pfu of HALo, and Ly6^{hl} (Ly6C^{hi}CD11b^{+}Ly6G^{-}) and Ly6C^{lo} (Ly6C^{lo}CD11b^{+} Ly6G^{-}) monocytes in the lung were measured by flow cytometry at day 2 post-infection.

(B) Mice were infected as in (A), and Ly6C^{hi} monocyte and neutrophil (Ly6C^{lo}Ly6G^{+}CD11b^{+}) influx was measured by flow cytometry at day 2 post-infection.

(C) Mice were infected as in (A), and viral titer in the lung was determined by plaque assay at day 3 post-infection. Titers were below the limit of detection at day 2.

(D) Gene expression in the lung of animals from (B) was determined by qPCR at day 2 post-infection. (B) and (D) show mean ± SD for n = 3 animals. (C) shows mean ± SD for n = 5 animals. (A) shows a representative FACs plot. **indicates significance of $p < 0.01$ using unpaired t test.

KEY RESOURCE TABLE

REAGENT or RESOURCE	SOURCE	IDENTIFIER
Antibodies		
CD3-APC (145-2C11)	BD	Cat#553066; RRID:AB_398529
CD19-APC (1D3)	BD	Cat#550992; RRID:AB_398483
CD11c-V450 (HL3)	BD	Cat#560521; RRID:AB_1727423
CD11c-PE-Cy7 (HL3)	BD	Cat#561022; RRID:AB_2033997
NK1.1-APC (PK136)	BD	Cat#550627; RRID:AB_398463
Ly6G-V450 (1A8)	BD	Cat#560603; RRID:AB_1727564
Ly6C-PerCP-Cy5.5 (AL-21)	BD	Cat#560525; RRID:AB_1727558
CD11b-PE (M1/70)	BD	Cat#561689; RRID:AB_10893803
B220-APC (RA3-6B2)	BD	Cat#561880; RRID:AB_10897020
CD45-APC (30-F11)	BD	Cat#561018; RRID:AB_10584326
SiglecF-BV421 (E50-2440)	BD	Cat#562681; RRID:AB_2722581
CD8-PerCP-Cy5.5 (53-6.7)	BD	Cat#551162; RRID:AB_394081
CD4-APC (GK1.5)	eBioscience	Cat#17-0041-82; RRID:AB_469320
CD103-APC (2E7)	eBioscience	Cat#17-1031-82; RRID:AB_1106992
EpCAM-PE-Cy7 (G8.8)	eBioscience	Cat# 25-5791-80; RRID:AB_1724047
CD31-PerCP-eFluor 710 (390)	eBioscience	Cat#46-0311-80; RRID:AB_1834430
MHC Class II (I-A/I-E) eFluor 450 (M5/114.15.2)	eBioscience	Cat#48-5321-82; RRID:AB_1272204
FasL-APC (MFL3)	eBioscience	Cat#17-5911-82; RRID:AB_10717074
CCR2-APC (475301)	R&D Systems	Cat#FAB5538A; RRID:AB_10645617
Influenza M2 (E10) conjugated to alexa 647	Bourmakina and García-Sastre, 2005	N/A
mouse anti-NP (HT-103)	Kerafast	Cat#EMS010; RRID:AB_2728685
rabbit polyclonal anti-NS1 (1-73)	Solórzano et al., 2005	N/A
rabbit β-Actin mAb HRP Conjugate	Cell signaling	Cat#5125; RRID:AB_1903890
Fc block	BD	Cat#553142; RRID:AB_394657
Bacterial and Virus Strains		
PR8: A/PR/8/34 (H1N1)	Extensively passaged lab strain	N/A
HALo: A/Viet Nam/1203/04 (H5N1) lacking the multibasic cleavage site	Steel et al., 2009	N/A
Cal09: A/California/04/09 (H1N1)	Hai et al., 2010	N/A
delNS1: A/PR/8/34 (H1N1) delNS1	García-Sastre et al., 1998b	N/A
PR8 NS1 R38A/K41A: A/PR/8/34 (H1N1)NS1 R38A/K41A	Talon et al., 2000	N/A
Chemicals, Peptides, and Recombinant Proteins		
Poly(I:C) HMW	Invivogen	Cat#tlrl-pic
R848	Invivogen	Cat#tlrl-r848
Universal type I IFN	PBL Interferon	Cat#11200-2
rmM-CSF	R&D Systems	Cat#416-ML
Dispase	BD	Cat#354235

REAGENT or RESOURCE	SOURCE	IDENTIFIER
Antibodies		
Collagenase type 4	Worthington	Cat#LS004209
DNase I	Sigma	Cat#D4527
LMA agarose	Lonza	Cat#50081
eFluor 455UV viability dye	eBioscience	Cat# 65-0868-18
AccuCount Particles	Spherotech	Cat#ACFP-70-10
Halt Protease and Phosphatase Inhibitor Cocktail	Thermo	Cat#78440
Critical commercial Assays		
EZNA total RNA kit	Omega	Cat#R6834-02
RNase-free DNase	Omega	Cat#E1091
Maxima Reverse Transcriptase and oligo-dT	Thermo	Cat#EP0743
LightCycler 480 SYBR Green I Master Mix	Roche	Cat#04887352001
Alexa Fluor 647 Protein labeling kit	Thermo	A20173
GoTaq Flexi DNA Polymerase	Promega	Cat#M8297
Experimental Models:Organisms/Strains		
C57BL/6J	Jackson	Cat#000664
Ifnb^{mob}: B6.129-*Ifnb1*^{tm1Lky}/J	Jackson	Cat#010818
Ifnar1$^{-/-}$	Müller et al., 1994	N/A
Stat2$^{-/-}$	Park et al., 2000	N/A
Oligonucleotides		
See Table S1		N/A
Recombinant DNA		
BAC clone RP24-363P1	BACPAC	Cat#RP24-363P1
pACYC177 backbone	NEB	Cat#E14151S
ACN cassette	Wu et al., 2008	N/A
DTx: PGKneolox2DTA	Soriano, 1997	Addgene#13443